

U-Net based Semantic Segmentation of Kidney and Kidney Tumours of CT Images

Benjamin Bracke and Klaus Brinker

Hamm-Lippstadt University of Applied Sciences, Marker Allee 76-78, 59063 Hamm, Germany

Keywords: Medical Image Segmentation, Semantic Segmentation, Kidney Tumours Segmentation, U-Net, Deep Learning, Transfer Learning, Hyperparameter Optimization.

Abstract: Semantic segmentation of kidney tumours in medical image data is an important step for diagnosis as well as in planning and monitoring of treatments. Morphological heterogeneity of kidneys and tumours in medical image data is a major challenge for automatic segmentation methods, therefore segmentations are typically performed manually by radiologists. In this paper, we use a state-of-the-art segmentation method based on the deep learning U-Net architecture to propose a segmentation algorithm for automatic semantic segmentation of kidneys and kidney tumours of 2D CT images. Therefore, we particularly focus on transfer learning of U-Net architectures and provide an experimental evaluation of different hyperparameters for data augmentation, various loss functions, U-Net encoders with varying complexity as well as different transfer learning strategies to increase the segmentation accuracy. We have used the results of the evaluation to fix the hyperparameters of our final segmentation algorithm, which has achieved a high segmentation accuracy for kidney pixels and a lower segmentation accuracy for tumor pixels.

1 INTRODUCTION

In 2020, more than 430,000 kidney tumours were diagnosed worldwide, nearly 40% resulted in death (Sung et al., 2021). Medical imaging techniques such as computed tomography (CT) play a central role in the diagnosis of kidney tumours as well as in planning and monitoring of treatment steps. Currently, analysing medical image data for precise localization and segmentation of kidney- and kidney tumours tissue is a manual and time-consuming process performed by radiologists (S. Kevin Zhou, 2020). Therefore, image segmentation techniques that can recognize related features in medical image data and assign a specific class (e.g. background, kidney or tumour) to each pixel could support the work of radiologists by automatically pre-segmenting the image data. However, the morphological heterogeneity of medical image data has been a major challenge for automatic image segmentation methods for a long time.

In recent years, major progress has been made in machine learning, which has also led to new and more powerful image segmentation methods based on artificial neural networks (Litjens et al., 2017), such as the deep learning U-Net architecture presented by Ronneberger et al. U-Nets are encoder-decoder architectures based on fully Convolutional-Neural-Networks (FCN) that combine a contractive

path for learnable feature extraction and an expansive path with skip connections between encoder and decoder for learnable upscaling of the extracted features (Ronneberger et al., 2015). In the past, U-Nets have been successfully used for segmentation of medical image data and in some applications have even been able to achieve better segmentation accuracy than radiologists (Litjens et al., 2017).

This paper picks up on the success of U-Nets and aims to develop a segmentation algorithm for semantic segmentation of kidney tissue and kidney tumours tissue from 2D CT image data. To achieve this objective, we will focus on transfer learning of existing and pre-trained U-Net architectures as well as on the optimization of its so-called hyperparameters, which are not trained automatically but have to be set manually. Therefore, we investigate in detail how different hyperparameters related to the data augmentation, loss function, U-Net encoders and transfer learning affect the segmentation accuracy.

In the following, we first introduce the considered dataset as well as different methods considered in the optimization of the U-Net hyperparameters. Then, the effects of the introduced methods on the segmentation accuracy are evaluated and discussed using empirical experiments, while the best methods will be included in our proposed segmentation algorithm. Finally, a conclusion is given.

2 MATERIAL AND METHODS

In this section, we will start with a description of the considered dataset and explain necessary adjustments and pre-processing steps. Afterwards, we present different methods considered in the optimization of the U-Net hyperparameters, which concern data augmentation, a suitable loss function for segmentation tasks and transfer learning of a U-Net architecture.

2.1 KiTS19 Dataset

The data used in this paper is derived from the "Kidney Tumor Segmentation 2019 (KiTS19)" dataset (Heller et al., 2019), which was released as a training dataset as part of a Grand-Challenge¹ under the creative commons license CC BY-NC-SA on March 15, 2019. It includes three-dimensional computed tomography images (CT volumes) of 210 patients who underwent nephrectomy at the University of Minnesota Medical Center. This dataset provides three-dimensional ground truth segmentations which assign the voxels of a CT volume to either the "kidney", "tumour" or "background" class, depending on the represented tissues. The CT volumes and segmentations have a spatial resolution of 512x512 voxels along the x- and y-dimensions, while the number of acquisition slices (z-dimension) varies between patients.

2.2 Pre-processing

We conducted some adjustments and pre-processing on the KiTS19 dataset, which are briefly explained in the following. Since this paper focuses on two-dimensional semantic segmentation, individual transverse CT images were extracted from the acquisition slices of each patient's three-dimensional CT volume. As a result, a total of 45,424 individual CT images were extracted from all 210 CT volumes, of which the majority ($\approx 64\%$) only contained the background class. About 23.4% of the images contained the classes background and kidney while approx. 11.5% contained all classes background, kidney and tumour. About 1.1% only contained the classes background and tumour. The high number of CT images containing only the background class does not provide further information about kidneys or tumours to the segmentation algorithm and could instead negatively impact training success and increase training run times. Consequently, most of these CT images were removed and only 1% (at least one image) per CT volume were retained. As a result of this filtering, only around 37% (16,795) of the extracted CT images remain. As the

¹<https://kits19.grand-challenge.org/>

number of acquisition slices of the patient CT volumes varies, the number of extractable CT images differs per patient. As a result, patients with many CT images would have a greater influence in training and in evaluation than patients with fewer CT images. To balance the influence of patients and avoid this bias, each CT image was weighted by a specific parameter. This parameter is equivalent to the inverse of the extracted and filtered number of CT images of a patient. During preprocessing, the intensity windows of the CT images were first clipped to [-125,225] Hounsfield units to achieve high contrast for the soft tissue of the abdomen and then normalized to the interval [0,1]. Also, the resolution of the CT images were reduced from 512x512 pixels to 256x256 pixels to decrease the processing time in the training process. All CT images were divided into training, validation, and test data on the patient level. From a total of 210 patients, 74 patients ($\approx 35\%$) were designated as test dataset, 116 patients ($\approx 55\%$) as training dataset and 20 patients ($\approx 10\%$) as validation dataset. Altogether, the test dataset provides a total of 5,494 CT images, the training dataset a total of 9,590 CT images, and the validation dataset a total of 1,711 CT images.

2.3 Data Augmentation

A major limiting factor when training artificial neural networks is the amount of available training data. The KiTS19 training dataset provides only a limited number of training data and consequently only low variability, which may lead to problems in training, such as overfitting and an overall poor generalization performance. Access to further training data with ground truth segmentations matching the topic of this paper is limited, so data augmentation techniques are used to artificially increase the variability of the training data by modifying them using various transformations. For this purpose, a data augmentation pipeline was developed, which combines spatial transformation methods like flipping, rotation, elastic transformation, grid distortion, crop or pad as well as intensity transformations like brightness-, contrast-, gamma adjustments, blurring, adding noise or compression artefacts. Data augmentation is performed dynamically for each CT image during the training process. Which transformation methods are used for data augmentation is determined randomly per image with a probability of 50% per transformation method. To prevent including only augmented images, the proportion of data augmentation can be specified by a hyperparameter. We will empirically evaluate this hyperparameter to determine the best proportion of data augmentation in terms of segmentation accuracy.

2.4 Loss Functions

Another important hyperparameter in training of artificial neural networks is the loss function, which quantifies the deviation between the networks prediction and the ground truth and should be minimized during the training process. A common problem in medical image data segmentation is the handling of class imbalances. The proportion of pixels that a kidney or tumour represents in a CT image is usually very small, resulting in a skewed distribution in favour of background pixels. Under these circumstances, a careful selection of a loss function that takes the unbalanced pixel distribution of each class into account is crucial. Therefore, we consider different loss functions and empirically evaluate which loss function is best suited in terms of segmentation accuracy for the purpose of this paper.

2.4.1 Cross Entropy

When cross entropy (CE) is used as a loss function for segmentation tasks, a loss is determined between predictions (p) and ground truth (g) for each pixel (i) and then averaged over all pixels (N). The cross entropy does not consider the class imbalance problem mentioned earlier. Therefore, we also consider a weighted cross entropy (WCE), which weights the pixel losses of each class (c) differently. The weighting parameters (w_c) of each class are calculated using the "Median-Frequency-Balancing" (Eigen andergus, 2014).

$$CE = -\frac{1}{N} \sum_{i=1}^N \sum_{c=1}^C g_{i,c} \cdot \log(p_{i,c}) \quad (1)$$

$$WCE = -\frac{1}{N} \sum_{i=1}^N \sum_{c=1}^C w_c \cdot g_{i,c} \cdot \log(p_{i,c}) \quad (2)$$

2.4.2 Dice Loss

We also investigate the dice loss (Sudre et al., 2017) function based on the Sørensen-Dice coefficient (DSC), which characterises the overlap between the prediction (p) and ground truth (g) and is therefore robust to different pixel proportions of the classes (c). Furthermore, we want to consider focusing of the dice loss similar to the Focal-Tversky loss (Abraham and Khan, 2018). Focusing is done by a γ -parameter, which exponentiates the dice loss for each class respectively. The effects of focusing are shown in Figure 1. Essentially, with a γ -value < 1 , the loss is higher for images with dice coefficients > 0.5 , which allows focusing on images that are easy-to-segment (Abraham and Khan, 2018). The opposite case is true

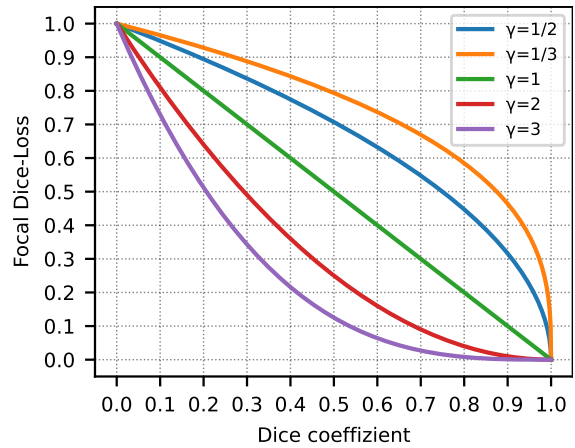


Figure 1: Focusing effects of the Focal-Dice loss compared to the dice coefficient. A focusing of $\gamma = 1$ corresponds to the unfocused Dice loss.

for a γ -value > 1 and allows focusing on harder-to-segment images. Both focusing cases will be empirically evaluated in this paper.

$$DSC_c = \frac{2 \sum_{i=1}^N p_{i,c} g_{i,c}}{\sum_{i=1}^N p_{i,c} + \sum_{i=1}^N g_{i,c}} \quad (3)$$

$$Dice Loss = \sum_{c=1}^C (1 - DSC_c) \quad (4)$$

$$Focal-Dice Loss = \sum_{c=1}^C (1 - DSC_c)^\gamma \quad (5)$$

2.5 Transfer-learning

Due to the limited amount of training data, this paper focuses on transfer learning and uses pre-trained Convolutional-Neural-Networks as a base model for the U-Net encoder. Which base model is best suited as a U-Net encoder will be evaluated empirically. For this purpose, we analyse how different variants of the ResNet architecture (He et al., 2015) like ResNet18, ResNet34, ResNet50 and ResNet101, which differ mainly in complexity due to a different number of convolutional layers, affect the segmentation accuracy. These pre-trained ResNet models have already learned a general feature extraction representation from the large ImageNet dataset, so only an optimization of the feature extraction with respect to the application field of this paper is required by re-training some layers. How far the optimization by re-training certain layers affects the segmentation accuracy will also be evaluated empirically. The U-Net decoder, which is designed to expand symmetrically to the stages of the ResNet architecture, is initialized randomly and must therefore be retrained each time.

2.6 Implementation

The segmentation algorithm with the previously described methods was implemented in Python 3.9.4, with the help of the libraries Tensorflow 2.4.1 and Numpy 1.20.1. The used U-Net architectures derive from the library Segmentation Models 1.0.1² and data augmentation was done with the libraries Albumentations 0.5.2 and OpenCV 4.5.2. The experiments for evaluation were performed on an Ubuntu 18.04 server with four Nvidia RTX 2080TI graphics cards, 128GB memory and two Intel Xeon Silver 4110 CPUs.

3 EVALUATION

In this section, we evaluate how the different considered methods for the U-Net architecture and hyperparameters for training affect the segmentation accuracy. First, we describe the performed evaluation approach. Then, the evaluation results of the considered methods and the results of the final segmentation algorithm are presented.

3.1 Approach

To determine how the different considered methods for the U-Net architecture and training hyperparameters affect the segmentation accuracy, several empirical experiments are conducted. Testing all possible combinations of the hyperparameters would be computationally too extensive, so instead we followed a stepwise approach.

For this purpose, all hyperparameters were first set manually as shown in Table 1. Starting from these initial hyperparameters, only one hyperparameter was evaluated at a time in sequential experiments. Dependencies between hyperparameters require careful consideration of the experimental sequence. Therefore, we first evaluated the hyperparameter of the data augmentation proportion to minimize early overfitting effects during the experiments, especially when training more complex U-Net encoders. The hyperparameter for the data augmentation proportion was then included in the second experiment, in which we evaluate the optimal loss function. Following the same approach, we decided to determine the optimal U-Net encoder and the hyperparameters for transfer learning in the last two experiments. All evaluated hyperparameters were then combined to train a final segmentation algorithm. During the experiments, different U-Net models were trained with a learning rate of

²https://github.com/qubvel/segmentation_models

Table 1: Initialization hyperparameters of the experiments.

Data Aug. Proportion	Loss Function	U-Net Encoder	Re-Trained Layers
0%	Dice Loss	ResNet34	from Stage 3

10^{-5} , a batch size of 24 CT images and a relatively short training period of 50 epochs to further reduce the computational cost. Afterwards, the segmentation accuracy for each model was evaluated using supervised pixel-based evaluation metrics over the entire validation dataset. We mainly focused on the evaluation metrics dice coefficient, recall and precision, that consider the classification cases of true positive (TP), false positive (FP), and false negative (FN) of each pixel in the segmented image with respect to the ground truth image (Taha and Hanbury, 2015). To minimize variations that may occur due to random influences in the training process, each experiment was repeated four times, and the mean and standard deviation of the metrics were used for evaluation.

$$\text{Dice coefficient} = \frac{2TP}{2TP + FP + FN} \quad (6)$$

$$\text{Recall} = \frac{TP}{TP + FN} \quad (7)$$

$$\text{Precision} = \frac{TP}{TP + FP} \quad (8)$$

3.2 Hyperparameter Optimization

In the following, the evaluation results of each hyperparameter experiment are presented and it is briefly mentioned which hyperparameter is used for the following experiment. A more detailed discussion is given in section 4.

3.2.1 Impact of Data Augmentation Proportion

The aim of the first experiment was to determine how different data augmentation proportions affect the segmentation accuracy. For this purpose, several U-Net models were trained using different data augmentation proportions $p \in [0\%, 25\%, 50\%, 75\%, 80\%, 90\%, 100\%]$. The data augmentation proportion $p=0\%$ is equivalent to no data augmentation.

Considering the results of the evaluation metrics, dice coefficient in Figure 2 and recall in Table 2, a clear trend can be seen. With increasing data augmentation proportion from $p=0\%$ to $p=75\%$, an improvement in segmentation accuracy can be observed. This improvement is particularly noticeable for the tumour class, where an approximately 13.5% higher dice coefficient and approximately 25.2% higher recall is achieved. In contrast, only minor fluctuations are observed for the kidney and background classes, which

Table 2: Evaluation results of recall and precision for the analyzed data augmentation proportions.

Class		Data Augmentation Proportion						
		0%	25%	50%	75%	80%	90%	100%
Recall	Background	99.9% ±0.0	99.9% ±0.0	99.9% ±0.1	99.9% ±0.1	99.9% ±0.0	99.9% ±0.0	99.9% ±0.0
	Kidney	87.3% ±0.4	87.7% ±0.5	87.1% ±1.0	88.1% ±0.8	88.0% ±0.6	87.2% ±1.1	87.2% ±0.4
	Tumour	51.7% ±2.3	69.8% ±3.0	75.6% ±1.0	76.9% ±2.6	75.2% ±2.4	74.8% ±1.8	77.0% ±1.7
Precision	Background	99.7% ±0.0	99.8% ±0.0	99.8% ±0.0	99.8% ±0.0	99.8% ±0.0	99.8% ±0.0	99.8% ±0.0
	Kidney	93.5% ±0.3	94.1% ±0.4	93.9% ±0.4	94.0% ±0.2	93.7% ±0.3	93.9% ±0.3	94.2% ±0.2
	Tumour	63.7% ±0.9	64.3% ±2.3	61.7% ±1.9	65.4% ±3.1	65.3% ±0.9	64.8% ±3.3	64.5% ±2.1

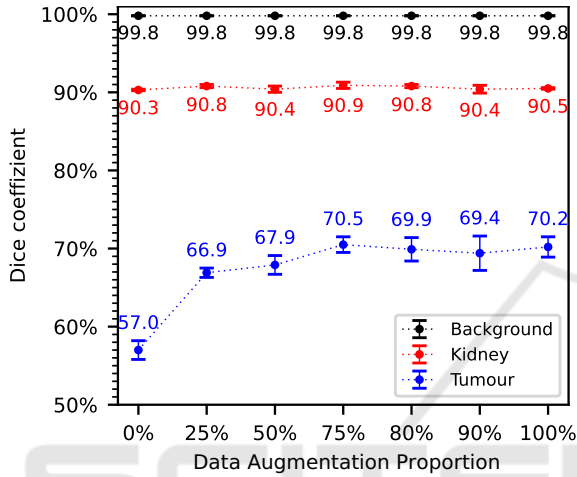


Figure 2: Evaluation results of the dice coefficient for the analyzed data augmentation proportions.

show no clear improvement in segmentation accuracy. At even higher data augmentation proportions of $p > 75\%$, no further improvement in segmentation accuracy is noticeable for the tumour class. Rather, a saturation of the dice coefficient at around 70% and for recall of around 75% to 77% is noticeable. There are only minor fluctuations in the evaluation results of the precision metric with partly high standard deviations, which do not indicate a clear trend.

According to these results, a data augmentation proportion of $p=75\%$ is selected as a hyperparameter for the following experiments as well as for the final segmentation algorithm.

3.2.2 Impact of Loss Function

The aim of the second experiment was to determine the effect of different loss functions on the segmentation accuracy. For this purpose, various U-Net models were trained using different loss functions in the training process. The influence of cross entropy versus weighted cross entropy was evaluated with weighting parameters of 0.02 for the background class, 1.0 for the kidney class and 1.5 for the tumour class. We also evaluated the influence of the dice loss on the

segmentation accuracy and whether focusing the dice loss with varying γ -values of $g \in [\frac{1}{2}, \frac{1}{3}, 2, 3]$ is useful.

The evaluation results of this experiment with respect to the dice coefficient are shown in Figure 3 as well as the results for recall and precision in Table 3. Comparing the evaluation results of the loss function cross entropy with those of the weighted cross entropy, the weighted cross entropy achieves higher recall results of about 3.9% for the kidney class and about 7.5% for the tumour class. In contrast, the other evaluation metrics show a significantly worse segmentation accuracy of the weighted cross entropy compared to the cross entropy. This is particularly noticeable in the dice coefficient, which is approximately 6.6% lower for the kidney class, and for the precision metric, which is approximately 15.8% lower. For the tumour class, there is only a slight improvement of about 1.5% in the dice coefficient with the weighted cross entropy, but also a significantly lower precision of about 3.7%. Comparing the evaluation results of the dice loss with the focused variants of the dice loss to easy-to-segment images ($\gamma = \frac{1}{2}$ and $\gamma = \frac{1}{3}$), only slight differences in segmentation accu-

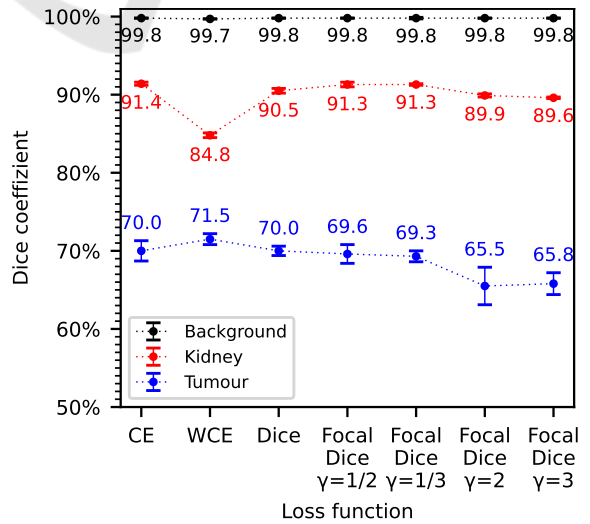


Figure 3: Evaluation results of the dice coefficient for the analyzed loss functions.

Table 3: Evaluation results of recall and precision for the analyzed loss functions.

	Class	CE Loss	WCE Loss	Dice Loss	Focal-Dice Loss			
					$\gamma = \frac{1}{2}$	$\gamma = \frac{1}{3}$	$\gamma = 2$	$\gamma = 3$
Recall	Background	99.9% \pm 0.0	99.4% \pm 0.0	99.9% \pm 0.0	99.9% \pm 0.0	99.9% \pm 0.0	99.8% \pm 0.0	99.8% \pm 0.1
	Kidney	89.0% \pm 0.3	92.9% \pm 0.7	87.4% \pm 1.0	88.4% \pm 0.7	88.4% \pm 0.4	87.3% \pm 0.4	86.6% \pm 0.2
	Tumour	69.4% \pm 0.8	76.9% \pm 1.5	77.9% \pm 1.0	73.4% \pm 0.8	73.7% \pm 2.1	66.5% \pm 3.2	67.0% \pm 2.0
Precision	Background	99.8% \pm 0.0	99.9% \pm 0.0	99.8% \pm 0.0	99.8% \pm 0.0	99.8% \pm 0.0	99.7% \pm 0.0	99.7% \pm 0.0
	Kidney	93.8% \pm 0.1	78.0% \pm 0.5	93.9% \pm 0.5	94.2% \pm 0.1	94.4% \pm 0.3	92.6% \pm 0.1	92.7% \pm 0.3
	Tumour	70.5% \pm 1.8	66.8% \pm 0.7	63.6% \pm 1.3	66.1% \pm 2.4	65.4% \pm 1.4	64.6% \pm 1.7	64.6% \pm 1.5

racy can be observed. These are mainly evident in a slightly better dice coefficient, recall and precision of the kidney class regarding the focused loss variants, but also in a slightly worse dice coefficient and recall of the tumour class. In general, recall and precision of the tumour class are more balanced for the focused loss variants than for the normal dice loss. Focusing on harder-to-segment images ($\gamma = 2$ and $\gamma = 3$) results in a significantly worse segmentation accuracy compared to the normal dice loss, as evidenced by approximately 4.3% lower dice coefficient and the approximately 10% lower recall of the tumour class.

Considering the more balanced recall and precision results and the high dice coefficient, the focused dice loss on easy-to-segment images ($\gamma = \frac{1}{2}$) is chosen as a hyperparameter for the following experiments as well as for the final segmentation algorithm.

3.2.3 Impact of U-Net Encoder

The aim of the third experiment was to determine the effects of different U-Net encoders of varying complexity in terms of segmentation accuracy. Therefore, various U-Net models were trained using four different Convolutional-Neural-Networks of the ResNet architecture as a basis for the U-Net encoder, including the ResNet18, ResNet34, ResNet50, and ResNet101.

Considering the results of the evaluation metrics dice coefficient in Figures 4 as well as recall and precision in Table 4, a trend is noticeable that with

Table 4: Evaluation results of recall and precision for the analysed U-Net encoders.

	U-Net Encoder	Background	Kidney	Tumour
Recall	ResNet18	99.9% \pm 0.0	87.7% \pm 1.1	66.4% \pm 2.2
	ResNet34	99.9% \pm 0.0	88.1% \pm 1.0	75.5% \pm 1.8
	ResNet50	99.9% \pm 0.0	88.8% \pm 0.7	74.4% \pm 3.4
	ResNet101	99.9% \pm 0.0	89.6% \pm 0.7	79.9% \pm 1.6
Precision	ResNet18	99.8% \pm 0.1	94.4% \pm 0.4	67.0% \pm 3.4
	ResNet34	99.8% \pm 0.0	94.5% \pm 0.2	65.3% \pm 2.6
	ResNet50	99.8% \pm 0.0	93.9% \pm 0.3	69.9% \pm 2.0
	ResNet101	99.8% \pm 0.0	94.6% \pm 0.3	70.9% \pm 1.8

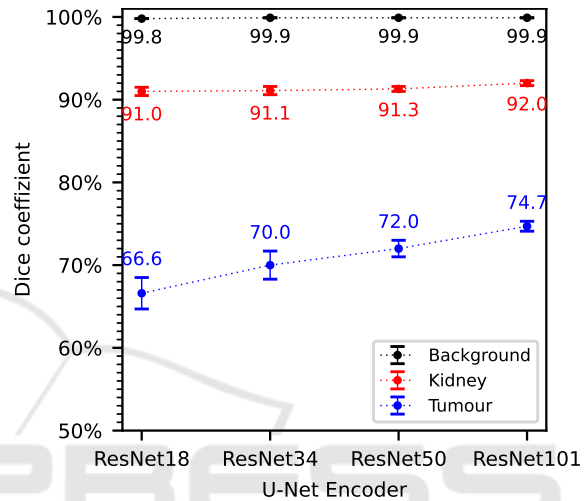


Figure 4: Evaluation results of the dice coefficient for the analysed U-Net encoders.

increasing complexity of the U-Net encoder an improvement in segmentation accuracy can be observed. This improvement in segmentation accuracy is again particularly noticeable in the tumour class, where the dice coefficient increased by an average of 2.7% with increasing complexity of the U-Net encoder. Recall improves by about 12.6% for the ResNet101 compared to the ResNet18, whereas precision increases by just 2.9%. For the kidney class, there is only a slight improvement in segmentation accuracy with increasing complexity of the U-Net encoder, while no significant changes occur for the background class.

According to these results, a U-Net encoder based on the most complex ResNet101 architecture is chosen as a basis for the following experiments as well as for the final segmentation algorithm.

3.2.4 Impact of Transfer-learning

The aim of the fourth experiment was to determine how the optimization of the pre-trained U-Net encoder (ResNet101) by re-training different numbers of layers affects the segmentation accuracy. To evaluate this, various U-Net models were trained in which

Table 5: Evaluation results of recall and precision for different numbers of re-trained encoder layers.

Class		Re-Trained Encoder Layers from:					
		All	Stage 1	Stage 2	Stage 3 Unit 1	Stage 3 Unit 12	Stage 4
Recall	Background	99.9% \pm 0.0	99.9% \pm 0.0	99.9% \pm 0.0	99.9% \pm 0.0	99.9% \pm 0.1	99.9% \pm 0.0
	Kidney	91.5% \pm 0.8	91.4% \pm 0.5	91.3% \pm 1.0	90.0% \pm 0.2	90.0% \pm 0.2	89.5% \pm 0.5
	Tumour	80.0% \pm 2.4	82.4% \pm 1.4	81.3% \pm 0.8	78.3% \pm 4.1	79.8% \pm 0.2	71.5% \pm 0.6
Precision	Background	99.9% \pm 0.0	99.9% \pm 0.0	99.9% \pm 0.0	99.8% \pm 0.1	99.9% \pm 0.0	99.8% \pm 0.0
	Kidney	95.4% \pm 0.2	95.5% \pm 0.1	95.0% \pm 0.3	95.0% \pm 0.2	94.6% \pm 0.4	94.4% \pm 0.2
	Tumour	76.8% \pm 2.1	75.3% \pm 0.2	75.8% \pm 3.3	72.4% \pm 1.5	63.6% \pm 3.1	68.4% \pm 3.3

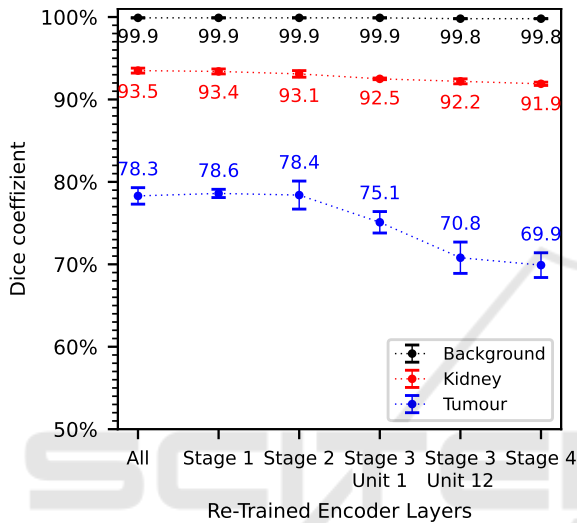


Figure 5: Evaluation results of dice coefficient for different numbers of re-trained encoder layers.

the neuron weights of several encoder layers were frozen to prevent them from being adjusted during the training process. First, a model is trained in which all encoder layers are re-trained and then models in which the encoder layers starting from ResNet-Stage 1, Stage 2, Stage 3 Unit 1 (Unit = Residual Block), Stage 3 Unit 12 and Stage 4 are re-trained.

Considering the results of the evaluation metrics dice coefficient in Figure 5 as well as recall and precision in Table 5, a clear trend is noticeable. In general, the segmentation accuracy decreases with decreasing number of re-trained encoder layers. Larger differences occur in dice coefficient and precision when only the encoder layers from Stage 3 and above are re-trained, whereas similar results are obtained when all encoder layers or the encoder layers starting from Stage 1 or 2 are re-trained. This trend is especially noticeable in the tumour class, where an approximately 8.4% higher dice coefficient and precision as well as an approximately 8.5% higher recall are achieved when all encoder layers are re-trained compared to re-training only the encoder layers from Stage 4. For the kidney class, this decreasing trend is only noticeable

to a minor degree while for the background class it is hardly noticeable at all.

As a result, all encoder layers are re-trained for transfer learning of the final segmentation algorithm.

3.3 Final Segmentation Algorithm

The aim of the previously performed experiments was to determine the optimal hyperparameters for the final segmentation algorithm as well as the final training process. As a result, of our evaluation the final training should use a data augmentation proportion of $p=75%$ and a more focused variant of the dice loss on easy-to-segment images ($\gamma = \frac{1}{2}$). Also, we determined that the best transfer learning basis for the final segmentation algorithm should be a pre-trained ResNet101 encoder, where all encoder layers should be re-trained. The same hyperparameters for learning rate and batch size were used in the final training process as in the previous experiments. Due to a lower computational cost for the evaluation, the number of training epochs of the experiments was limited to 50, which was negligible for the final training. Therefore, the number of training epochs was extended to 150 to benefit from a longer training period. For the reasons explained in section 3.1, the final training process was also repeated four times and segmentation accuracy was evaluated using the averaged results of the evaluation metrics over the entire test dataset.

The evaluation result of the final segmentation algorithm is presented in Table 6 as well as in the confusion matrix in Figure 6. In addition, Figure 7 illustrates examples of the segmentation result. As can be seen in the clear diagonal of the confusion matrix, most of the pixels of the test dataset were seg-

Table 6: Evaluation results of dice coefficient, recall and precision for the final segmentation algorithm.

Metric	Background	Kidney	Tumour
Dice coeff.	99.9% \pm 0.0	94.7% \pm 0.1	84.5% \pm 0.4
Recall	99.9% \pm 0.0	94.8% \pm 0.1	81.2% \pm 1.0
Precision	99.9% \pm 0.0	94.6% \pm 0.3	88.1% \pm 0.4

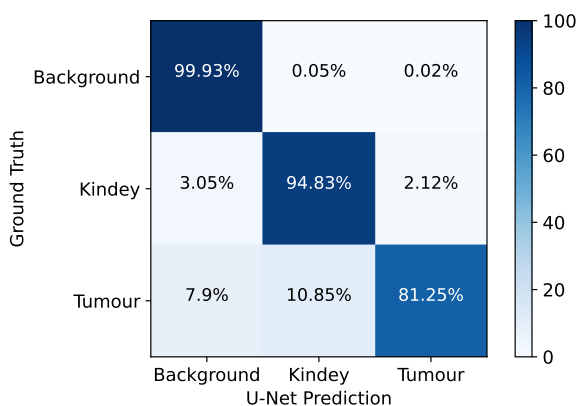


Figure 6: Normalized confusion matrix visualizing the segmentation accuracy of the final segmentation algorithm.

mented with high accuracy. However, significant differences in segmentation accuracy can be observed for the individual classes. With approximately 99.9% for the dice coefficient, recall and precision, the final segmentation algorithm achieved a very high segmentation accuracy for background pixels. A lower segmentation accuracy of about 94% for the dice coefficient, recall and precision was achieved for kidney pixels. According to the confusion matrix, only 3.05% were incorrectly predicted as background pixels and 2.12% as tumour pixels. A significantly lower segmentation accuracy was achieved for tumour pixels, resulting in only about 81.25% correctly predicted tumour pixels. In contrast, the precision of tumour pixels is significantly higher with approximately 88.1%. According to the confusion matrix,

the final segmentation algorithm misclassified a large proportion of tumour pixels of about 10.85% as kidney pixels and about 7.9% as background pixels.

4 DISCUSSION

The purpose of this paper was to develop a U-Net-based segmentation algorithm for automated semantic segmentation of kidneys and kidney tumours from 2D medical CT images. Therefore, we mainly focused on transfer learning and determined the optimal hyperparameters for the U-Net based segmentation algorithm in various sequential experiments to increase the overall segmentation accuracy.

4.1 Data Augmentation Proportion

First, we experimented with the hyperparameter for a different data augmentation proportion to investigate the influence on the segmentation accuracy. The results have shown that with increasing data augmentation proportion, a significant improvement in segmentation accuracy was achieved, especially for the tumour class. This trend was noticeable up to a data augmentation proportion of $p=75%$, after which no further improvements in segmentation accuracy occurred. The obtained results confirm the previously made assumption that the considered training dataset provides only a low variability, which can be significantly increased by data augmentation and is therefore highly recommended. Data augmentation pro-

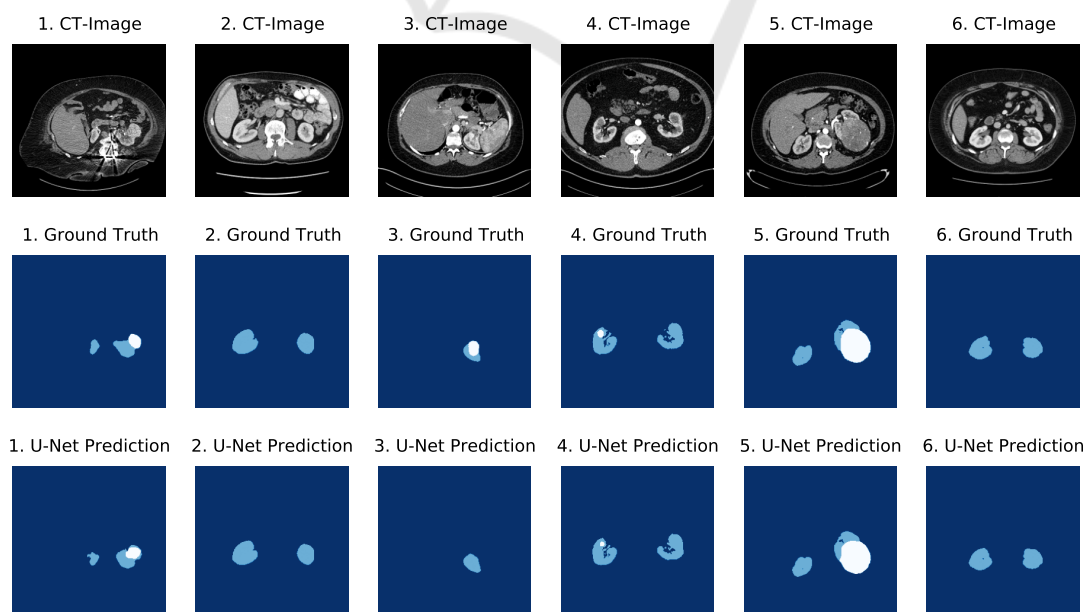


Figure 7: Examples of the segmentation results of the final segmentation algorithm. Dark blue regions represent the background class, light blue regions the kidney class and white regions the tumor class.

portions of $p > 75\%$ may have resulted in an excessive variability of the training data, preventing further improvements in segmentation accuracy in the limited number of training epochs of this experiment. Perhaps increasing the number of training epochs would produce larger differences. As a consequence of these results, we decided to select a data augmentation proportion of $p = 75\%$ as hyperparameter for the following experiments and for the final segmentation algorithm.

4.2 Loss Function

Second, we considered different loss functions to investigate the impact on segmentation accuracy. Originally, we expected that the weighting parameters would make the cross entropy more robust to unequal pixel distributions of the classes and hence improve the segmentation accuracy. Compared to the cross entropy, significantly higher recall values could be achieved with the weighted cross entropy, but also much lower precision and dice coefficients, especially for the kidney class. As a consequence of these ambiguous results, no clear improvement of the segmentation accuracy could be observed with the weighted cross entropy compared to the cross entropy. Perhaps the variation of the pixel distribution of a class between the CT images is too large, so that a fixed weighting parameter often causes an over- or under-weighting of the class, resulting in lower segmentation accuracy. Potentially, a dynamic weighting parameter that determines a weighting value for each class per CT image could improve accuracy. We also considered the dice loss and investigated whether it is useful to focus the dice loss on harder- or easy-to-segment images. Compared to the dice loss, focusing on harder-to-segment images did not improve segmentation accuracy. A possible reason for this could be the early convergence of the loss function (Figure 1), which could lead to very small loss changes towards the end of the training process, so that improvements in segmentation accuracy also converge. This would also explain why focusing on easy-to-segment images generally yields better results, as late convergence towards the end of the training process still leads to significantly larger loss changes. Compared to the dice loss, focusing on easy-to-segment images produced comparable or even better results. For the next experiments and the final segmentation algorithm, we selected the loss function that achieved the highest possible segmentation accuracy over all classes as well as the most balanced results across the considered evaluation metrics, which was true for the dice loss focusing on easy-to-segment images ($\gamma = \frac{1}{2}$).

4.3 U-Net Encoder

Third, we considered different U-Net encoder complexities using the ResNet architecture to investigate the influence on segmentation accuracy. The results show that as the encoder complexity increases, the segmentation accuracy also improves, especially for the tumour class. One possible reason is that a high encoder complexity can also learn a larger number as well as more complex features from the image data due to the larger number of convolutional layers, which seems to have an overall positive effect on segmentation accuracy. To investigate this effect in more detail, it is recommended to consider even more complex encoders, such as ResNet152. Due to the resulting increase in training time, no further investigations were performed in this paper and the most complex ResNet101 encoder for the U-Net architecture was selected for the following experiments as well as for the final segmentation algorithm.

4.4 Transfer-learning

In the fourth experiment, we re-trained different pre-trained encoder layers during transfer learning to investigate the influence on segmentation accuracy. In general, the results showed that the segmentation accuracy also decreased with a decreasing number of re-trained encoder layers, especially for the tumor class. In particular, the segmentation accuracy was significantly worse when only the encoder layers from stage 3 or onwards were re-trained. These results suggest that the already learned features of the encoder derived from the ImageNet dataset do not generalize sufficiently to this medical image dataset, so further optimization is required. This is especially true for features in the encoder layers of stage 2 and above, as inferior segmentation accuracy occurred primarily when these encoder layers were not re-trained. We decided to re-train all layers of the ResNet101 encoder for the final segmentation algorithm to achieve the best possible segmentation accuracy.

4.5 Final Segmentation Algorithm

Based on the previously evaluated hyperparameters, we trained our proposed final segmentation algorithm. It achieves high segmentation accuracy for background and kidney pixels, while segmentation accuracy for tumour pixels is lower, especially with respect to misclassifications as kidney pixels. A possible reason for the inferior segmentation accuracy of the tumour class could be the significantly lower occurrence of the tumour class in the training dataset.

Perhaps an adjustment or expansion, with equal proportions of tumour and kidney classes, could improve segmentation accuracy. Another possible reason could be an insufficient contrast between the pixel intensities of the tumour and kidney class, which would explain the more frequent confusion of tumour pixels with kidney pixels. Perhaps further pre-processing would be necessary to increase the contrast. In addition, further optimization of the hyperparameters, such as the learning rate, batch size, number of training epochs or the use of different base models as the U-Net encoders, could further improve the segmentation accuracy. Due to dependencies between hyperparameters, a different order in hyperparameter optimization could also affect segmentation accuracy, making grid or random search a potentially better but computationally more expensive alternative than sequential experiments. Moreover, including the third dimension of CT volumes using 3D U-Nets could also improve segmentation accuracy.

A statement about the medical suitability of the final segmentation algorithm could not be made. This would require more test data as well as a comparison of the achieved segmentation accuracy with other segmentation algorithms, e.g. with the results of the KiTS19-Challenge participants. This comparison was not made because the participants followed a different, three-dimensional evaluation approach and used a different test dataset whose ground truth annotations are not publicly available.

5 CONCLUSION

In this paper, we presented a U-Net based segmentation algorithm, for automatic semantic segmentation of kidneys and kidney tumours from 2D medical CT images. For this purpose, we mainly focused on transfer learning of a pre-trained U-Net architecture and the optimization of its hyperparameters, which include data augmentation, loss function, U-Net encoder complexity and transfer learning. Experimental results show that the segmentation accuracy can be significantly improved by extensive data augmentation, a dice loss with focus on easy-to-segment images, a complex ResNet as U-Net encoder and the re-training of many encoder layers during transfer learning. A final segmentation algorithm could be trained as a result of this hyperparameter evaluation, which achieved a high segmentation accuracy for kidney pixels ($\approx 94\%$ dice coefficient), whereas the segmentation accuracy for kidney tumour pixels was lower ($\approx 84\%$ dice coefficient) with an increased probability of misclassifications as kidney pixels. Compar-

ing the results with other segmentation algorithms is pending to further investigation. A promising direction for further research that might improve segmentation accuracy is the use of more training data, additional hyperparameter optimizations, minimization of hyperparameter dependencies as well as an adaptation to a 3D U-Net-based approach.

ACKNOWLEDGEMENT

This work has been supported by the European Union and the federal state of North-Rhine-Westphalia (EFRE-0801303).

REFERENCES

- Abraham, N. and Khan, N. M. (2018). A Novel Focal Tversky loss function with improved Attention U-Net for lesion segmentation.
- Eigen, D. and Fergus, R. (2014). Predicting Depth, Surface Normals and Semantic Labels with a Common Multi-Scale Convolutional Architecture.
- He, K., Zhang, X., Ren, S., and Sun, J. (2015). Deep Residual Learning for Image Recognition.
- Heller, N., Sathianathan, N., Kalapara, A., Walczak, E., Moore, K., Kaluzniak, H., Rosenberg, J., Blake, P., Rengel, Z., Oestreich, M., Dean, J., Tradewell, M., Shah, A., Tejpaul, R., Edgerton, Z., Peterson, M., Raza, S., Regmi, S., Papanikolopoulos, N., and Weight, C. (2019). The KiTS19 Challenge Data: 300 Kidney Tumor Cases with Clinical Context, CT Semantic Segmentations, and Surgical Outcomes.
- Litjens, G., Kooi, T., Bejnordi, B. E., Setio, A. A. A., Ciompi, F., Ghafoorian, M., van der Laak, J. A. W. M., van Ginneken, B., and Sánchez, C. I. (2017). A survey on deep learning in medical image analysis. *Medical Image Analysis*, 42:60–88.
- Ronneberger, O., Fischer, P., and Brox, T. (2015). U-Net: Convolutional Networks for Biomedical Image Segmentation.
- S. Kevin Zhou (2020). *Handbook of Medical Image Computing and Computer Assisted Intervention*. Elsevier.
- Sudre, C. H., Li, W., Vercauteren, T., Ourselin, S., and Cardoso, M. J. (2017). Generalised Dice overlap as a deep learning loss function for highly unbalanced segmentations.
- Sung, H., Ferlay, J., Siegel, R. L., Laversanne, M., Soerjomataram, I., Jemal, A., and Bray, F. (2021). Global Cancer Statistics 2020: GLOBOCAN Estimates of Incidence and Mortality Worldwide for 36 Cancers in 185 Countries. *CA: A cancer journal for clinicians*, 71(3):209–249.
- Taha, A. A. and Hanbury, A. (2015). Metrics for evaluating 3D medical image segmentation: analysis, selection, and tool. *BMC Medical Imaging*, 15(1):29.